


Handbook
for
Generic Photonic IC Design

Editors: Meint Smit and Xaveer Leijtens

4-4-2026

 *Handbook for generic photonic IC design*, by the *Photonic Integration group*, Technische Universiteit Eindhoven, is licensed under a Creative Commons “Attribution-NonCommercial-NoDerivatives 4.0 International” license.

We traced the ownership of all figures used as far as we could. However, if you are a copyright owner and believe we used your work without permission, please contact us at coordinator@jeppix.eu.

Chapter 11

Polarization Rotators and Converters

JOS VAN DER TOL

Polarization is a special property of guided waves, since only two stable polarization states (polarized modes) are normally found in waveguides, usually referred to as TE-like and TM-like modes. Any light input with a polarization state that does not match these modes will result in both modes being excited, leading to an undefined (and changing) polarization in the waveguides. In this chapter, and in Chapter 27, it will be described how to work with this aspect of guided waves. The essential function needed to manipulate polarization in a Photonic Integrated Circuit (PIC) is the polarization converter. This is a device that couples energy from the TE-like mode into the TM-like mode, and vice versa. The operation principles of this device will be explained, and its properties will be worked out. In Chapter 27 the polarization converter will be used in various application circuits that make use of the polarization. In the current chapter you will find:

- A descriptions of polarization states
- The concept of a polarization converter
- Properties of birefringent materials
- Properties of birefringent waveguide sections
- Tolerance and optical bandwidth of polarization converters

Strictly speaking a polarization converter is a composite building block: it consists of a polarization rotation section between two junctions. The basic building block is the polarization rotator. Because it is not very useful without the junctions we describe it here in its application as polarization converter.

11.1 Polarization effects in PICs

In Section 2.3 the nomenclature of the TE- and TM-polarizations is introduced in the context of reflection and refraction at the interface between two media. Since waveguiding in dielectric waveguides depends on total internal reflections, the polarization

dependence described there will also apply to the guided modes. In a planar slab waveguide pure TE- and TM-modes can be found, since either the electric field (for “Transverse Electric”, TE), or the magnetic field (for “Transverse Magnetic”, TM) polarization is parallel to the interfaces of the waveguide. However, this is different for channel waveguides. There all three spatial dimensions will have electric and magnetic field components. This results from the total reflection occurring in both the “vertical” (defined as normal to the chip surface) and “horizontal” (in-plane) directions. Since the overall geometry is planar, and the mode fields are therefore predominantly polarized in the horizontal or vertical directions, the modes can often still be described as TE-like and TM-like (or quasi-TE and quasi-TM). However we will see in this chapter that this is not always so, and useful effects can be obtained with waveguide structures that support modes which are polarized differently.

TE-mode
TM-mode

polarization dependence Let us first however consider what effects these two polarized modes can have on the operation of PICs, and why this can be problematic (or beneficial). The two polarized modes have different propagation constants. Usually the TE-like mode has a higher propagation constant than the TM-like mode of the same order. This means, e.g., that the TE-mode has a higher confinement in the high-index region of the waveguide and, therefore, also a lower propagation loss. It also implies that beating between the modes can become an issue if there are points in the optical circuit where they couple. Coupling points can easily appear at the input and output ports of the optical circuit, at bends and transitions and even in straight sections due to sidewall roughness. Since the beating depends on mode excitation, on wavelength and on temperature, the resulting performance of the PIC will vary with those parameters. Furthermore, the two polarized modes have different evanescent fields, which results in different interactions with the interfaces and the claddings. The TE-mode has a stronger evanescent field in the horizontal direction and is, therefore, more sensitive to nearby structures and bends in the waveguide. The TM-mode, with a stronger evanescent field in the vertical direction, is more sensitive to, e.g., doped layers above and below the waveguide layer, resulting in higher absorption losses. On the other hand, the TM-mode is better for interacting with materials on top of the waveguide, as is needed for sensing applications or for magneto-optic (non-reciprocal) devices. More on these points can be found in chapter 27. Finally, the material used in InP-based PICs in itself also results in polarization sensitive behaviour. In electro-optical modulators (see chapter 17) the linear electro-optic effect (the Pockels effect) is used. This effect depends on the direction of the electric field of the modes, hence the polarization, and thus leads intrinsically to a polarization dependent device. Also the active materials used in lasers, SOAs and electro-absorption modulators (see chapters 14-16) are mostly polarization dependent, as they often contain strained quantum wells.

All of these effects result in polarization dependent operation of PICs, which is problematic if the input state of polarization is not exactly aligned to one of the polarized modes. And even if this perfect alignment can be achieved, any polarization coupling in the optical circuit can lead to degradation of performance. There are ways to combat these problems, and these will be described in chapter 27.

However, the existence of two polarized modes also presents opportunities. The TE and TM-modes can support different functions in the same circuit. One example is the use of polarization multiplexing, in which both modes are independently manipulated to carry separate communication channels. More examples of how polarization can be used will be given in chapter 27.

In order to control the polarization in a PIC it is essential to be able to transfer energy from one polarized mode to the other, and vice versa. This is done with a polarization

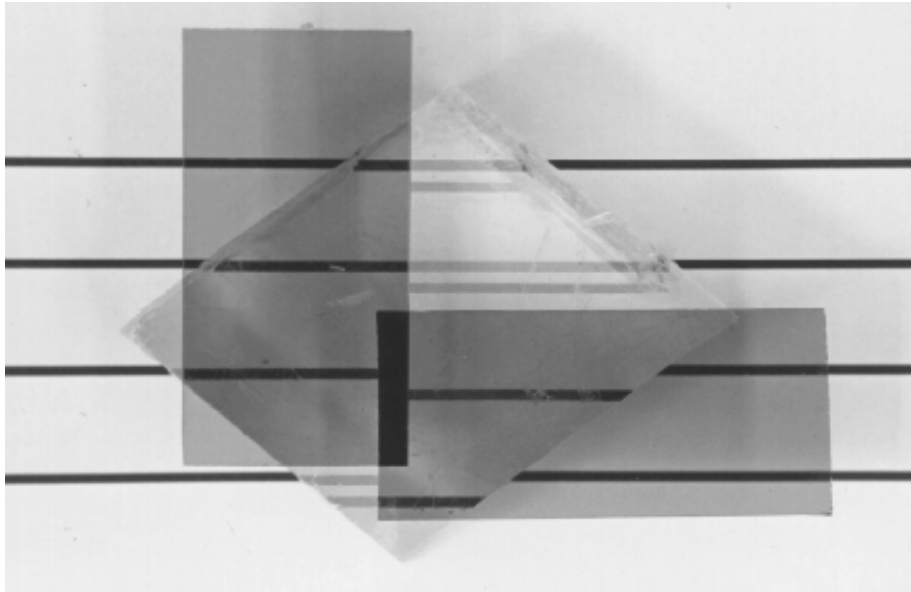


Figure 11.1: Images viewed through a calcite crystal. Two polaroid analysers are placed with their transmission axes at right angles to each other (with one aligned parallel to the optical axis). The ordinary and the extraordinary waves give separate images. (From S. Kasap, “Optoelectronics and Photonics: Principles and Practices”)

converter. It is sometimes also, but less accurately, described as polarization rotator. In the context of this chapter the first term will be used for the full device, while the latter refers to the waveguide section used in it. The remainder of this chapter will describe how this function is obtained in the generic platform.

*polarization
converter
polarization
rotator*

11.2 Polarization conversion

In bulk optics polarization can be manipulated using retardation plates; optically transparent devices made out of birefringent material. The most used are halfwave plates (HWP) and quarter wave plates (QWP). Their operation is relevant for the polarization converters on the InP-platform, so it is useful to explain these first.

*halfwave plate
quarter wave plate*

Birefringence occurs in anisotropic materials. The refractive index of such a material depends on the direction of the oscillating electric field of a light wave. In a uniaxial material the z-axis is usually chosen along the deviating crystal orientation (called the “optical axis”), with the x- and y-axes being equivalent. A light beam polarized along the z-axis is then called the “extraordinary” wave, while those polarized along the other axes are the “ordinary” waves. One of the effects of this is, e.g., a double image from a piece of Icelandic spar (this is a transparent form of calcite, which is a birefringent crystal. See Fig. 11.1), resulting from the different refraction for ordinary and extraordinary waves.

*birefringence
uniaxial material
optical axis
extraordinary wave
ordinary wave*

In a retardation plate light is polarized at the input under an angle of 45° with the z-axis. In the birefringent material this wave then splits up in two separate independently propagating waves, one extraordinary and one ordinary, each carrying half of the optical power. Since the input is at normal incidence to the plate, there is no refraction visible, but the two waves do built up a phase difference. Let’s call the refractive in-

retardation plate

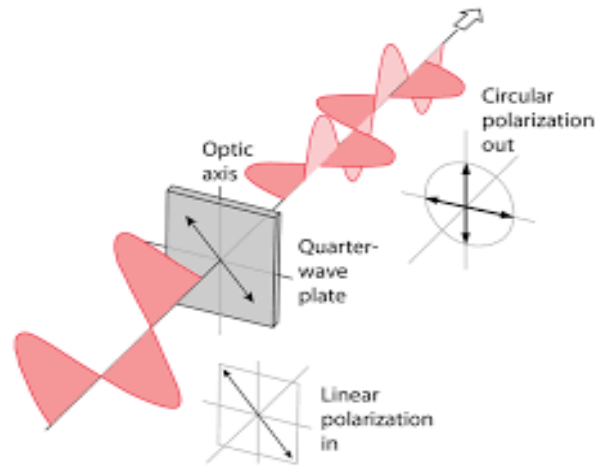


Figure 11.2: Operation of a QWP: transformation of a linear polarization into a circular one.

index for the ordinary wave n_o and that for the extraordinary one n_e . Then the phase difference $\Delta\phi$ after propagation over a length L becomes:

$$\Delta\phi = \frac{2\pi}{\lambda_0}(n_e - n_o)L \quad (11.1)$$

*circular
polarization
quarter wave plate*

With λ_0 the wavelength of light in vacuum. The operation of the retardation plate now depends on the value of this phase difference, and thus on the length of the propagation path through the birefringent material. For example, if the two waves are 90° out of phase at the exit of the plate, they combine into a circular polarized wave, in which the electric field follows a spiral path. This is depicted in Fig. 11.2. This retardation plate is then called a quarter wave plate (QWP), referring to the length being $1/4$ times the full beating length (for which $\Delta\phi = 360^\circ$).

half wave plate

Note that the operation can also be reversed: when the input wave has a circular polarization, the output will be linearly polarized at a 45° angle with respect to the z -axis. Another useful function, which actually is the analogue for the polarization converter, is obtained with $\Delta\phi = 180^\circ$. In that case the two waves in the birefringent material leave the plate with opposite phase difference as compared to the input. So one of them obtains a minus sign with respect to the other, and as a result they recombine to a wave polarized at an angle of -45° angle with respect to the z -axis, which means the resulting output wave is orthogonally polarized w.r.t. the input. In Fig. 11.3 this is shown. For reasons that will be obvious to the reader by now this device is known as a half wave plate (HWP).

*polarization
converter*

Together the QWP and the HWP make it possible to manipulate the state of polarization of a light beam. At the heart of these devices lies the material birefringence. And here appears a problem, when trying to implement such functions on the generic photonic integrated platform: InP is an isotropic material, as are usually the materials epitaxially grown on it. By including strain in the materials, using lattice mismatch, anisotropy can be obtained. This is however limited (too much strain will lead to damaged materials) and leads to an optical axis that is perpendicular to the chip surface, and thus normal and parallel to the electric fields of the TE- and TM-modes, while the operation of the retardation plates requires an optical axis at 45° angle. So how can we create the required type of birefringence to build a HWP (polarization converter) in

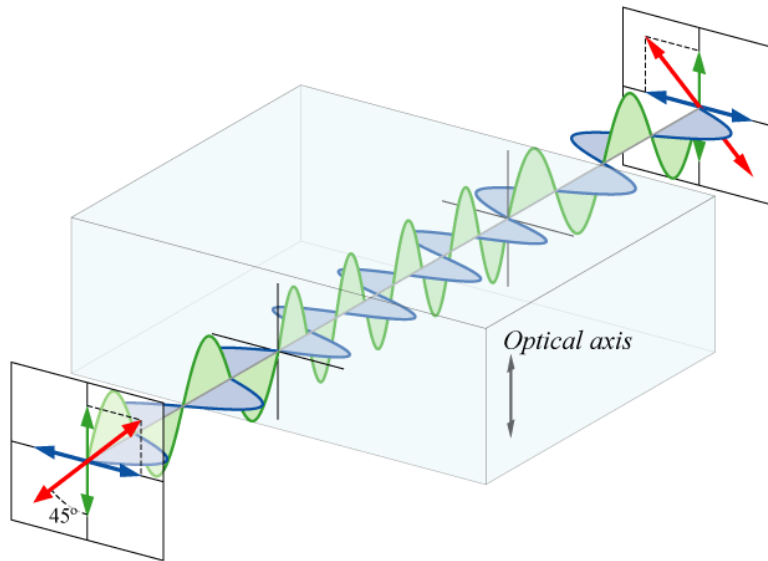


Figure 11.3: Operation of a HWP: transformation of a linear polarization into an orthogonal one

PICs? The answer is to make use of waveguide birefringence, the polarization dependent propagation that occurs due to the electromagnetic boundary conditions in the interaction with material interfaces surrounding the waveguide core. This is explained in the next section.

11.3 Waveguide birefringence¹

Transparent waveguides are used to guide the light on a PIC. Here we focus on the birefringence of these waveguides. The birefringence can be either enhanced, to be able to use it, or made as small as possible, to be able to neglect it. The main design parameters available for this are the geometrical dimensions of the waveguide: the width and the etch depth. Two types of waveguide are distinguished on the generic platform: shallowly and deeply etched waveguides. Shallow waveguides are etched 100 nm into the waveguide layer; deep waveguides are etched completely through. The birefringence, the difference in refractive index for the two orthogonal polarizations, is causing polarization dependent behaviour. In a waveguide, the modal birefringence, the difference in effective index ($\Delta N_{\text{eff}} = N_{\text{eff, TM}} - N_{\text{eff, TE}}$) that the propagating polarized modes experience, is caused by a different confinement of the light for the two polarizations, by different electromagnetic boundary conditions, and by the possible presence of material birefringence. These different causes of birefringence are discussed in Appendix 11.7D. Here we use waveguide birefringence in an asymmetric waveguide to obtain the operation of a retardation plate in a photonic integrated circuit.

*modal
birefringence*

¹This section is based on Section 2.2 in the PhD Thesis of Luc Augustin [161].

11.4 Sloped sidewall polarization converter

polarization converter The polarization converter (PC) consists of a waveguide with a straight and a sloped sidewall [178]. In such an asymmetric waveguide the modes cannot any longer be considered as “TE”- or “TM”-like, but instead their major field components will be tilted with respect to the surface of the chip, due to the electromagnetic boundary conditions. In this way the waveguide birefringence is influenced such that a rotated optical axis is obtained. The principle behind this structure is explained below. The processing of polarization converters requires additional process steps that will be discussed next. The description of the devices and the visualization will be based on the Jones-calculus, on Stokes-vectors and on the Poincaré-sphere. For readers not familiar with these entities introductions are given in the Appendices 11.7A, 11.7B and 11.7C of this chapter.

11.4.1 Principle²

polarization state The polarization converter using tilted birefringent modes is the integrated optical analogue of the half wave plate in bulk optics. As explained above, a half-wave plate has an ordinary and an extraordinary axis: two orthogonal modes can exist with differing propagation constants. When the axes are tilted with respect to the input polarization, both modes are excited and after propagating over a certain distance through the device, the two modes are out of phase and recombine to a different polarization state. The equivalent integrated device consists of a ridge waveguide with a straight and a sloped sidewall (Fig. 11.5). Polarization conversion can be obtained with a narrow waveguide having such a sloped interface. Due to the electromagnetic boundary conditions the sloped interface rotates the polarization of the modes. With a careful design the rotation will be 45°. In that case a TE-mode from a symmetric input waveguide equally excites the two rotated orthogonal modes. These modes propagate with different propagation constants. After half of the beat length the rotated modes recombine to a TM-mode in a symmetric output waveguide. In this way full conversion between TE and TM is possible. Since the device is reciprocal, a full conversion from TM to TE can be obtained in the same way. The waveguide is narrow, typically below 1 μm. This brings the sloped sidewall close to the field of the mode. Because of the ‘tilted’ boundary conditions, the hybrid (i.e., the mixing of pure TE- and TM-modes) nature of the modes is enlarged. Ideally this causes the modes to tilt for +45° and –45° respectively. Furthermore, the geometry of the waveguide causes a different propagation constant for the two modes. The angle of the sloped sidewall does not have to be 45° (in our case it is 54.7° with respect to the surface). The tilt angle of the modes for a certain slope angle is determined by the width. In Fig. 11.4 the tilt angle

tilt angle

$$\theta = \arctan(E_y/E_x) \quad (11.2)$$

Pointing vector is plotted as a function of the width of the polarization converter waveguide for the modes inside the converter. In this equation E_x and E_y are the average value over the mode field. It can be calculated from the fraction of the Pointing vector with horizontal or vertical electric field, respectively, integrated over the cross section. The mode solvers usually provide this number as “TE-fraction” or “TM-fraction”.

If light in a straight waveguide is coupled to the PC waveguide, both tilted modes are excited. After a half beatlength,

²This section is based on section 4.2 in the PhD Thesis of Luc Augustin [161].

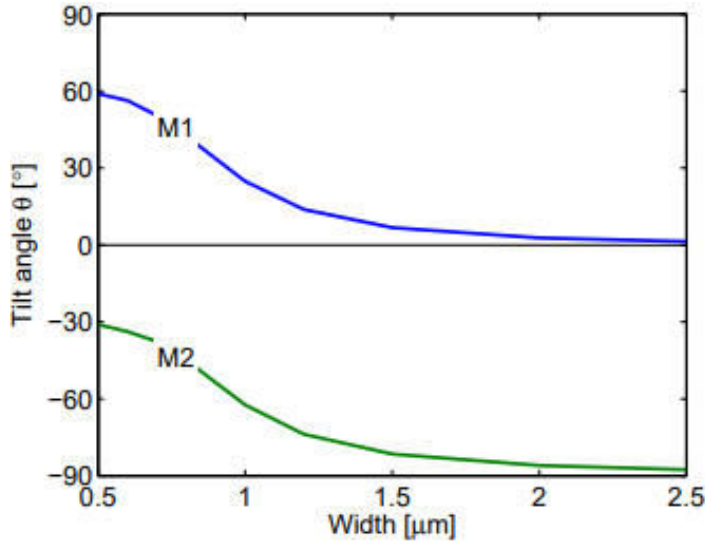


Figure 11.4: Tilt angle of the modes inside the PC as a function of waveguide width.

$$L_{\lambda/2} = \pi / (\beta_1 - \beta_2) \quad (11.3)$$

where β_n is the propagation constant of mode n, the modes are completely out of phase and recombine into the orthogonal polarization in a straight output waveguide. This is clarified in Fig. 11.5(b), where the propagation of modes M_1 and M_2 is shown over a length $L_{\lambda/2}$, corresponding to a phase difference $\phi = \pi$ rad.

11.4.2 Modeling

The properties of the conversion of the PC can be explained using Jones matrices (see [Jones matrix](#) Appendix 11.7A). The PC with length L creates a phase difference ϕ between the two orthogonal modes. In the coordinate system of the tilted modes, the transfer matrix T_{PC1} of the PC itself is:

$$T_{PC1} = \begin{bmatrix} 1 & 0 \\ 0 & e^{-j\phi} \end{bmatrix} \quad (11.4)$$

The directions of the electric field of the two modes inside the PC are in the regular coordinate system (normal along the y-axis):

$$M_1 = \begin{pmatrix} \sin(\theta) \\ \cos(\theta) \end{pmatrix}, \quad M_2 = \begin{pmatrix} \cos(\theta) \\ -\sin(\theta) \end{pmatrix} \quad (11.5)$$

The modes inside the PC are tilted over an angle θ with respect to the modes in the straight waveguide. The total transfer of the PC is obtained by a coordinate transformation. The tilted modes form the new basis for the calculations of the PC. The transfer with respect to the regular TE-TM modes is obtained by multiplication with a rotation matrix $R(\theta)$:

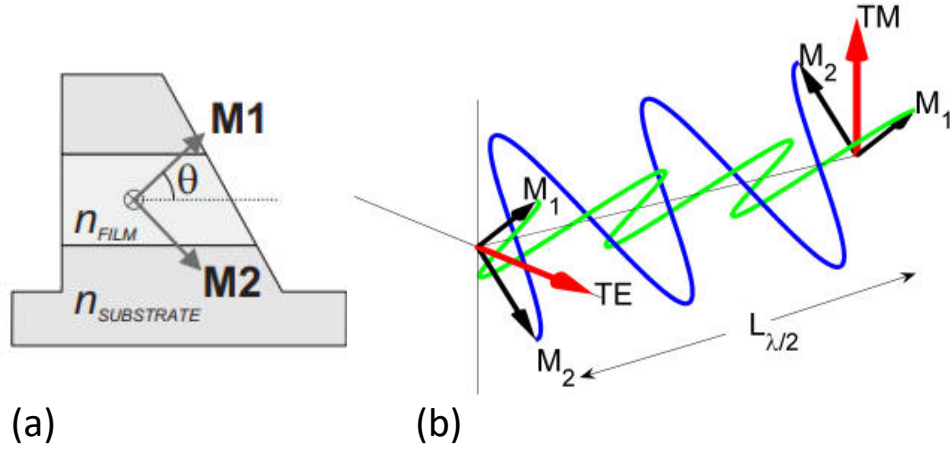


Figure 11.5: Principle of the integrated polarization converter. (a) Schematic cross section of the PC (b) Propagation of the modes.

$$R(\theta) = \begin{bmatrix} \cos(\theta) & \sin(\theta) \\ -\sin(\theta) & \cos(\theta) \end{bmatrix} \quad (11.6)$$

Fig. 11.6(a) shows the transformation to the new basis.

The transfer of the PC is:

$$T_{PC} = R(\theta)^{-1} T_{PC1} R(-\theta) \quad (11.7)$$

which is equal to

$$\begin{bmatrix} \cos(\theta)^2 + \sin(\theta)^2 e^{-j\phi} & \cos(\theta) \sin(\theta) (1 - e^{-j\phi}) \\ \cos(\theta) \sin(\theta) (1 - e^{-j\phi}) & \sin(\theta)^2 + \cos(\theta)^2 e^{-j\phi} \end{bmatrix} \quad (11.8)$$

For TE input, this yields an output E_2 :

$$E_2 = \begin{bmatrix} \cos(\theta)^2 + \sin(\theta)^2 e^{-j\phi} \\ \cos(\theta) \sin(\theta) (1 - e^{-j\phi}) \end{bmatrix} \quad (11.9)$$

conversion efficiency Which leads to the following expression for the conversion efficiency:

$$c = \frac{P_{\text{converted}}}{P_{\text{total}}} = 2[\cos(\theta) \sin(\theta)]^2 [1 - \cos(\phi)] \quad (11.10)$$

Poincaré sphere state of polarization SOP The operation of a polarization converter can be represented on the Poincaré sphere (explained in Appendix 11.7C). Every possible state of polarization (SOP) is described by a point on the surface of this sphere. The two intersections with the x-axis are the TE and the TM points, the intersections with the z-axis are left-handed and right-handed circular polarizations, and the intersection with the y-axis are oppositely 45° tilted linear polarizations. The polarization conversion from TE to TM consists of a rotation of π rad around an axis through the two stable polarization states in the converter section (which are ideally the oppositely 45° tilted linear polarizations). The rotation angle is

rotation angle

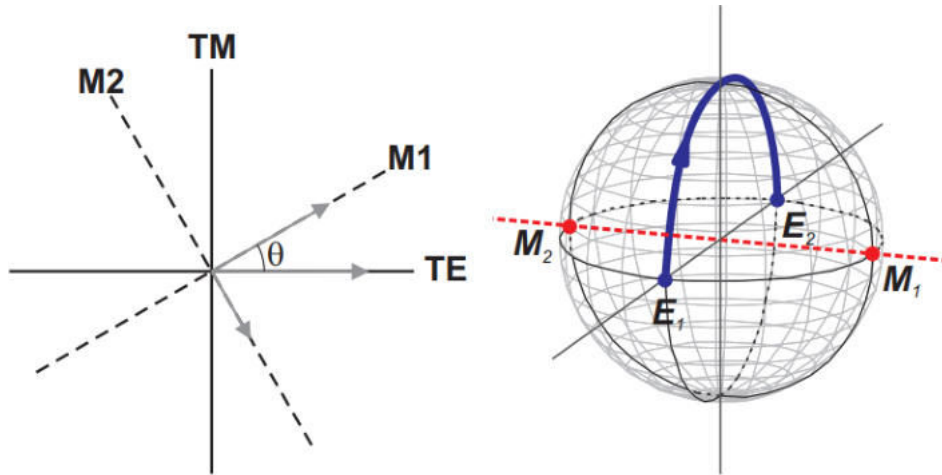


Figure 11.6: Visualization of the conversion. (a) Coordinate transformation to new basis for PC (b) Conversion of the PC plotted on the Poincare sphere.

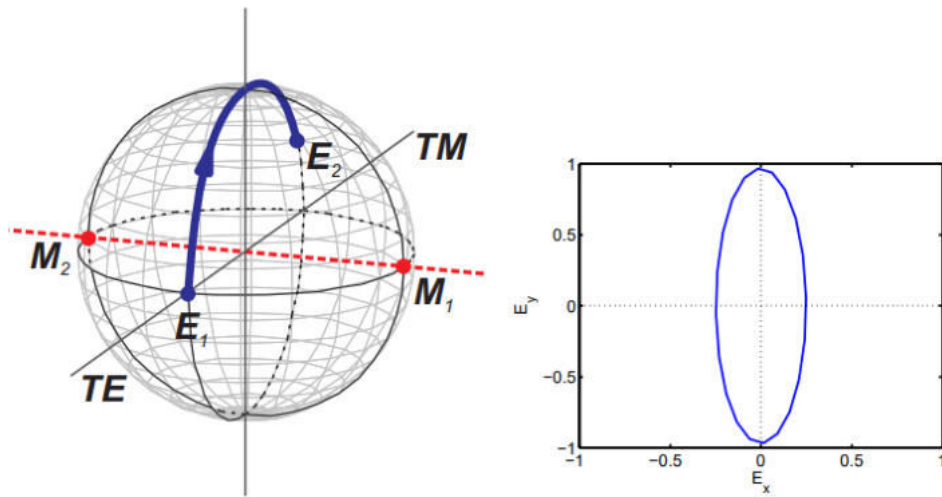


Figure 11.7: Incomplete conversion due to incorrect length. (a) Conversion of the PC plotted on the Poincare sphere (b) Output SOP

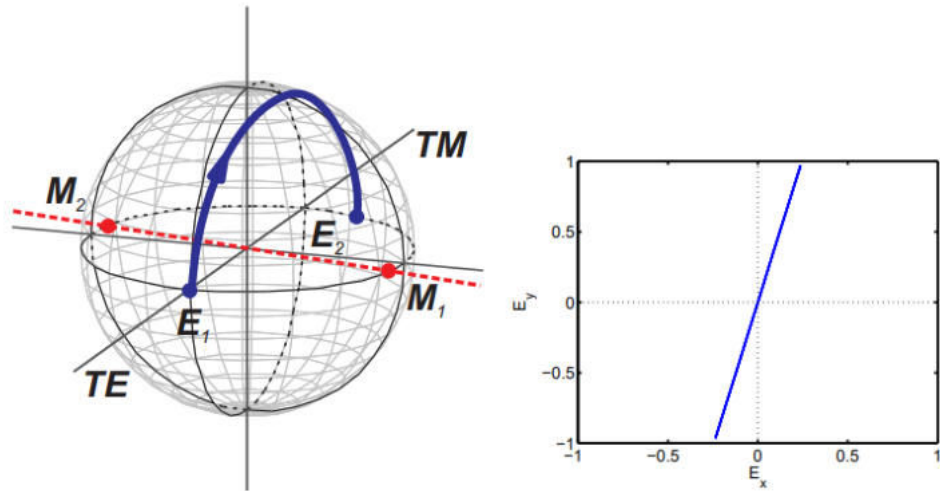


Figure 11.8: Incomplete conversion due to incorrect width. (a) Conversion of the PC plotted on the Poincare sphere (b) Output SOP

the phase shift between the two modes in the converter. The two stable modes are indicated with M_1 and M_2 . Propagation through the PC results in a rotation around the axis between these two points. In Fig. 11.6(b) the conversion from TE (E_1) to TM (E_2) in an ideal PC ($\theta = \pi/4$ and $\phi = \pi$) is shown. From the equations above it is clear that the amplitudes of the two components of E_2 depends on both the tilting angle θ and the phase difference ϕ . Incomplete conversion can therefore have two different causes:

- The PC has the correct width and therefore a required tilt angle θ of 45° , but the length is incorrect. At the output the modes are not exactly out of phase. This leads to an elliptical vertical polarization as shown in Fig. 11.7.
- The PC does not have the correct width; the tilt θ is not exactly 45° . After propagation over the beatlength, the two orthogonal modes are completely out of phase and result in a linear polarization. However they do not recombine to a polarization orthogonal to the input. This can be seen on the Poincare sphere in Fig. 11.8. The two stable modes in the structure in this case are not exactly on the $\pm 45^\circ$ points, but are on different points on the equator of the sphere, as indicated in Fig. 11.8(a).

The conversion of the PC is the ratio between the converted and the total power, in both examples the ratio is the same, but the output SOP is different. Thus the origin of the incomplete conversion cannot be discovered by regarding the output powers for one device. The θ , and thus the maximum possible conversion, can be obtained by a scan in length (i.e. a scan in ϕ).

11.4.3 Fabrication³

sloped sidewall bromine A sloped sidewall can be obtained with wet etching. Several solutions are possible. The cleanest etchant to use for this is bromine (Br_2), dissolved in methanol [179] to a very diluted solution (1:1500). $\text{Br}_2:\text{CH}_3\text{OH}$ etches both InP and InGaAsP and stops at the

³This paragraph is partially based on the PhD Thesis of Jeroen Bolk, sections 6.6.1 and 6.6.2. [147]

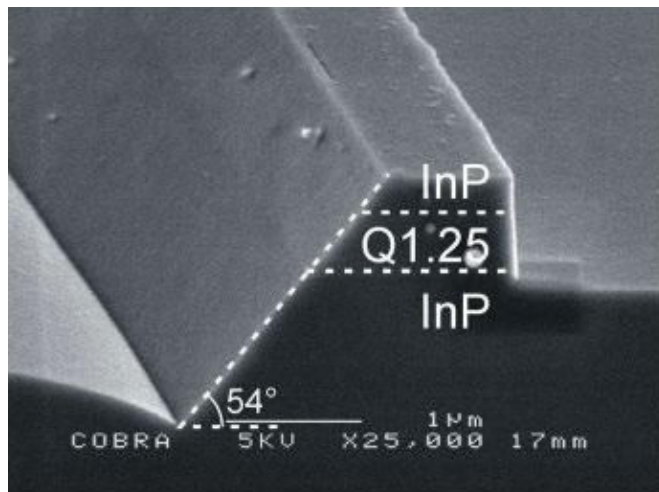


Figure 11.9: Smooth etch of quaternary and InP with $\text{Br}_2:\text{CH}_3\text{OH}$.

(111) planes for both, providing a slope angle of 54.7° with respect to the surface. This results in a very smooth surface (Fig. 11.9). Therefore this is the etchant of choice for the polarization converters.

To realize a polarization converter geometry with a sloped sidewall in a full integration process, the flow shown in Fig. 11.10 was developed. At the start of this process, a waveguide is defined, with a depth equal to the starting point of the slope. During step 1, the first lithography is performed to protect the polarization section with resist. During step 2, the combined resist and hard mask is used to realize the correct waveguide etch depth outside the polarization sections, after which the resist mask is removed. Step 3 will deposit a conformal 100 nm SiN layer on the entire sample using PECVD. During Step 4 the lithography is performed, which opens the polarization converter sections. After the dry etch of the dielectric mask in step 5, the polarization converter sections are open, while leaving a self-aligned spacer on the sidewall of the PC section. During step 6, the sloped sidewall is etched using diluted bromine methanol ($\text{Br}_2:\text{CH}_3\text{OH}$). This etch results in the slope of 54.7 degrees [160]. During the last step all dielectric material is removed from the sample with a BHF etch, which exposes the desired geometry.

11.5 Tolerance analysis of the Polarization Converter

As shown in Figs 11.7 and 11.8, in case of a deviation of a realized polarization converter from the optimal design two different errors can occur. The first is that the rotation (i.e., the phase shift) is different from the required π radians. The result is an elliptical SOP. The second possible error is that the tilting angle of the modes is different from 45° . In that case the final SOP is linear, (note that the linear polarization states are all on the equator of the Poincaré sphere), but it is rotated with respect to the TM-polarization. Of course, in practice these two errors will appear together when the realized device deviates in some way from the design.

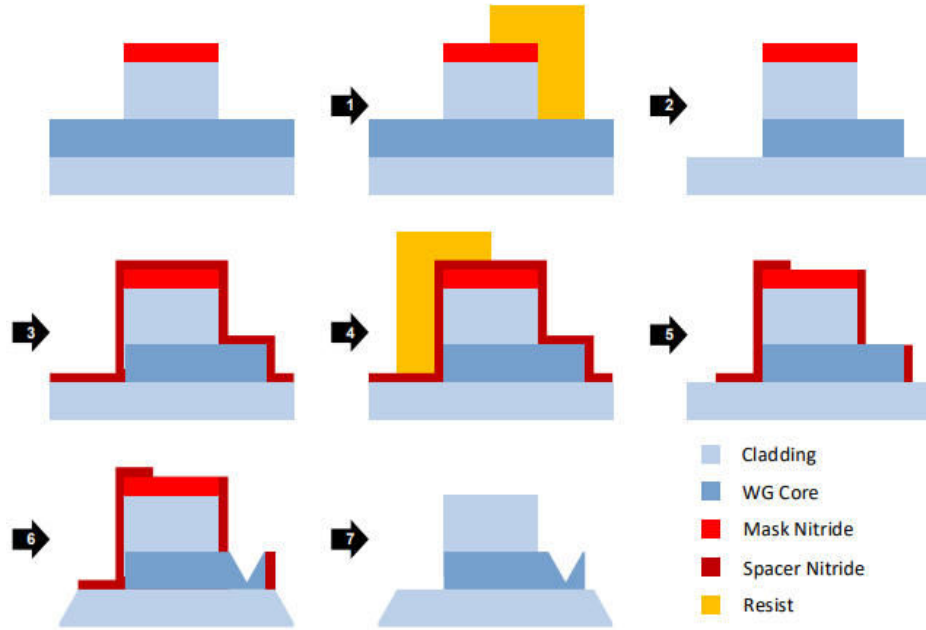


Figure 11.10: Process flow for a generic polarization converter in the TU/e technology platform

11.5.1 Theory

As was derived in Eq. 11.10, the conversion efficiency C of a polarization converter is given by the following formula:

$$\begin{aligned} C &= P_{\text{converted}}/P_{\text{total}} \\ &= 2\{\cos(\theta)\sin(\theta)\}^2\{1 - \cos(\phi)\} \end{aligned} \quad (11.11)$$

in which θ is the tilting angle of the modes and ϕ is the phase shift between them. Clearly, for a perfect converter $\theta = \pi/4$ rad and $\phi = \pi/2$ rad. If deviations occur with respect to these values, due to fabrication errors, changes in operational conditions or differences in material parameters, the change in conversion is approximated by

$$\Delta C = -4(\Delta\theta)^2 - 0.25(\Delta\phi)^2 \quad (11.12)$$

This is obtained with a Taylor series expansion. Since the first and third order expansion terms are zero, this equation is correct up to the fourth order. This suggests that the effect of errors in the tilting angle are more important than those in the phase shift. This will depend however on the actual value of the deviations. It will be shown below, with simulations and general argumentation, that indeed the tilting angle deviation is dominant in reducing the conversion efficiency.

11.5.2 Simulations

The polarization converter is investigated with the structure depicted in Fig. 11.11. As will be discussed below, the results obtained for this converter are representative for all other sloped sidewall polarization converters as well.

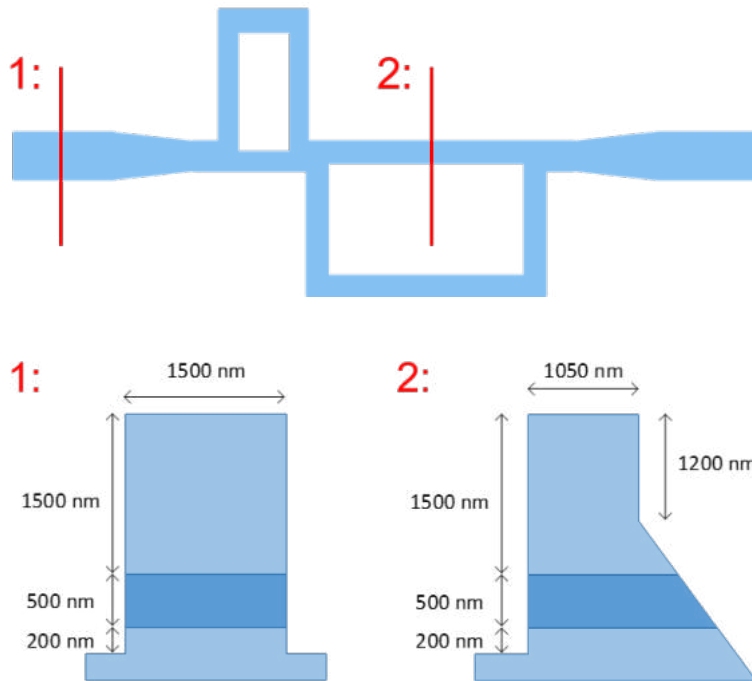


Figure 11.11: Example of a polarization converter, used for analysis of the tolerances. Top-down view of a double section (DS) version (left), and cross-sections at the marked intersections of waveguide (1) and polarization section (2).

The first important issue is the relative impact of the two possible deviations; the error on the tilt angle $\Delta\theta$ and the error on the phase shift $\Delta\phi$. Previous work [180], [161], has shown that the width of the converter section seems to be the most critical parameter. Hence, the modes in the polarization converter section are analysed as a function of the width deviation ΔW_{PC} with a FMM-mode solver [181]. $\Delta\theta$ and $\Delta\phi$ versus ΔW_{PC} are shown in Fig. 11.12.

A linear dependence of $\Delta\theta$ with ΔW_{PC} is found. The phase shift $\Delta\phi$ however has a quadratic dependence, leading to a minimum close to the design point for W_{PC} . As a consequence, for large negative values of ΔW_{PC} , i.e., when the converter waveguide is much smaller than designed, we can expect that $\Delta\phi$ would give the dominant error (if $\Delta\phi$ is larger than 4 times $\Delta\theta$, according to Eq. 11.12). However, in the region close to $\Delta W_{PC} = 0$, and for positive values, the tilting error clearly dominates. This raises the question if a minimum in the $\Delta\phi$ -curve close to the design width is a general property of sloped sidewall polarization converters. Simulations on other designs [180] show similar behaviour, thus suggesting the generality. This can be understood by considering the mechanism behind the tilting of the modes. The polarization of the modes is determined by the electromagnetic boundary conditions at the material interfaces of a waveguide cross section. Since most of these are either horizontal or vertical, TE- and TM-like modes are generally found. In the polarization converters the interface that is placed under an angle induces the tilting of the modes. To obtain the desired 45° tilting angle, despite the presence of the horizontal and vertical interfaces, some level of hybridization of the TE- and TM-modes is needed. Such hybrid modes require that the propagation constants of the modes are close together, which is therefore a necessary condition for a sloped sidewall polarization converter. Since the phase shift

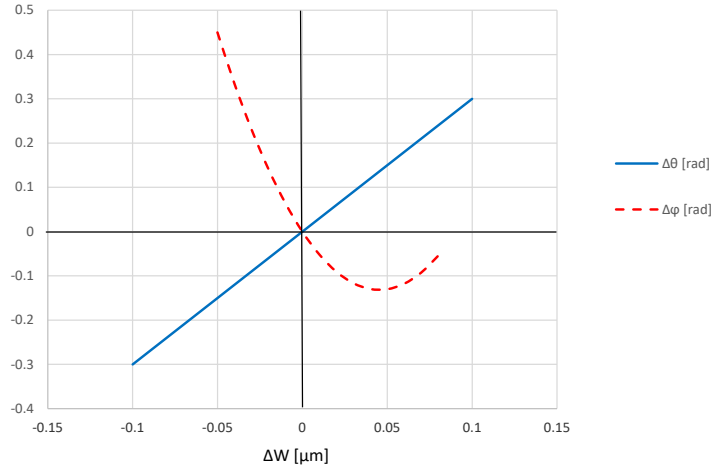


Figure 11.12: Error in θ and ϕ as a function of the waveguide width deviation.

between the modes is proportional to the difference in the propagation constants, this implies that a minimum in the phase shift will be found close to the optimal design of any sloped sidewall polarization converter. Fig. 11.13 shows the effect of the two errors on the simulated conversion. The theoretical result, based on Eq. 11.11, and added error contributions are very close together; underlining the validity of the analysis, i.e., higher order terms in the Taylor expansion (Eq. 11.12, using the results of Fig. 11.13) indeed have a small influence for these values of ΔW_{PC} . The contribution of the phase shift error $\Delta\phi$ is negligible, except for widths which are more than 30 nm smaller. Over the whole investigated width range the tilt angle error $\Delta\theta$ is dominant.

11.5.3 The Double-Section Polarization Converter

Double-Section Polarization Converter tolerance

The analysis above indicates that to improve the tolerance of the polarization converter a correction to the error in the tilting angle θ in particular must be made. It can be done by adding an extra section to the polarization converter, which corrects the tilting angle error. With the diagram in Fig. 11.14 this is illustrated. Although the the Double-Section Polarisation Converter is clearly a Composite Building Block we discuss it here because the analysis is so closely connected to that of the Single-Section PC.

The diagram shows a top view of the Poincaré sphere, with the polarization conversions indicated by the axes (shown as red dotted lines) around which the rotation of the SOP takes place, and the rotation trajectories themselves projected as blue straight (for the upper hemisphere) and dotted (for the lower hemisphere) lines perpendicular to the rotation axes. Here we will use the conversion from TE to TM as an example. Since these devices are reciprocal, the conclusions will also hold for the reverse conversion (TM to TE). If we allow the rotation to go halfway, i.e., around $\pi/2$ rad, the error in the tilting angle can be compensated with a rotation around an axis which is mirrored in the TE-TM axis. This second rotation would be on a circle that crosses the TM-point. To achieve this a second converter section is needed, in which the tilting angle is $-\theta$, so the modes there are oppositely tilted. Exactly such a relation is obtained for two polarization converter sections which have mirrored cross sections, as is illustrated in Fig. 11.15.

In practical realizations, it will be rather straightforward to obtain a mirrored cross section, as both sections will be simultaneously realized in the same material. Any devi-

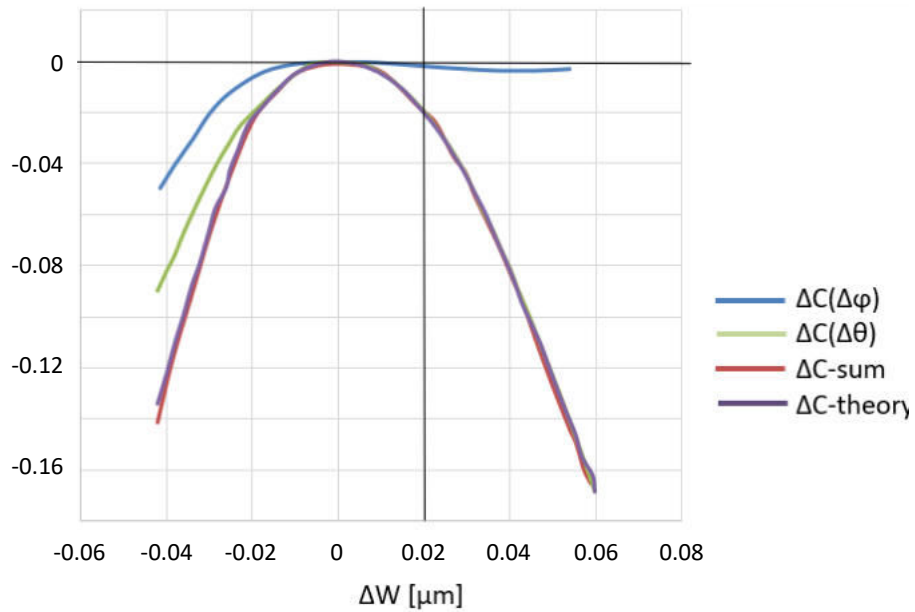


Figure 11.13: Change in conversion efficiency ΔC as a function of width deviation from contributions of the error on the tilt angle [$\Delta C(\Delta\theta)$], the error on the phase shift [$\Delta C(\Delta\phi)$], and their sum [$\Delta C\text{-sum}$], as compared with the theoretical values [$\Delta C\text{-theory}$]

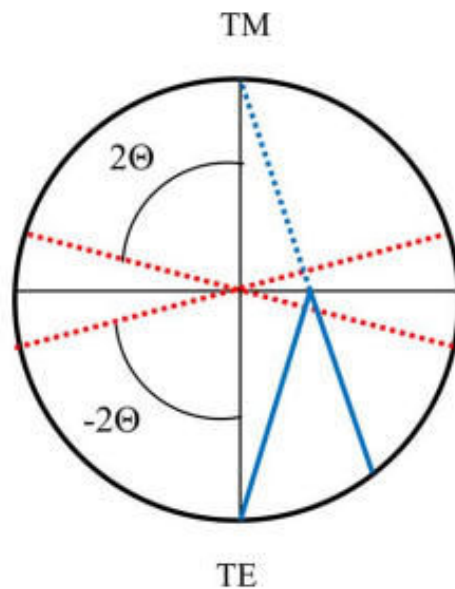


Figure 11.14: Projection on the equator plane of the Poincaré sphere. Red lines indicate the rotation axes, blue lines the rotation trajectories.

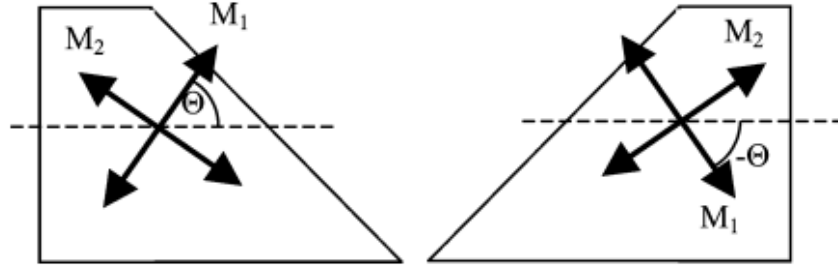


Figure 11.15: Mirrored cross section polarization converter leads to tilting angles of the modes with reversed sign. Note that the polarized modes M_1 and M_2 are always orthogonal.

ation in width and material composition can therefore be the same in both (but of course this depends on the processing chosen, e.g., if the width of the two sections is defined in the same lithographic step, as is the case is [180],[161]). However, because of the mirroring the second section will give a rotation of the SOP over the surface of the Poincaré sphere in the opposite direction, which means that a rotation angle of $3\pi/2$ rad is required to reach the TM-point. The tolerant polarization converter thus consists of two sections of different length; one has a length $L_{\lambda/4} = \pi/2(\beta_1 - \beta_2)$, while the other has a length which is thrice as long: $L_{3\lambda/4} = 3\pi/2(\beta_1 - \beta_2)$. The total length of a device is therefore twice the length of a single section device. Fig. 11.16(upper) shows the complete path of the SOP on the Poincaré sphere upon propagation through a device consisting of two mirrored sections with lengths adjusted to the required phase shifts. Fig. 11.16(lower) shows the schematic structure of the double section polarization converter.

Intuitively, one can understand the increased tolerance of the double section polarization converter as follows. Ideally, in each of the two sections the tilting angle is 45° . Both sections contribute equally to the polarization conversion (because the long mirrored section, with phase shift $3\pi/2$ rad between the modes, can be considered as having a phase shift $-\pi/2$ rad, so equal in magnitude to the phase shift in the short section). Thus, as any error on the tilt angle will be opposite in both sections, on average the tilt angle of 45° will be maintained in the full device.

Using the theory of section 11.4.2 the conversion efficiency of the double section polarization converter can be derived as

$$C = [\sin^6(\theta) \cos^2(\theta) + \sin^2(\theta) \cos^6(\theta)] \cdot [6 + 4 \cos(\frac{\phi}{2}) - 4 \cos(\frac{3\phi}{2}) + 2 \cos(2\phi)] + [\sin^4(\theta) \cos^4(\theta)] \cdot [-4 - 8 \cos(\frac{\phi}{2}) - 8 \cos(\phi) + 8 \cos(\frac{3\phi}{2}) - 4 \cos(2\phi)] \quad (11.13)$$

Again, for an optimal converter $\theta = \pi/4$ and $\phi = \pi$. Performing a similar Taylor series expansion as before we can arrive at the change in C :

$$\Delta C = -0.25(\Delta\phi)^2 \quad (11.14)$$

which indeed shows that the error in θ is compensated for up to the fourth order, while only the error in ϕ remains. The dependence of the conversion efficiency as a function of θ (assuming a negligible error in ϕ) can be plotted for the original and for the tolerant version of the polarization converter (Fig. 11.17).

These curves reveal the origin of the tolerant behavior: for the two section device a plateau appears around the optimal value, indicating that the error in tilting angle can

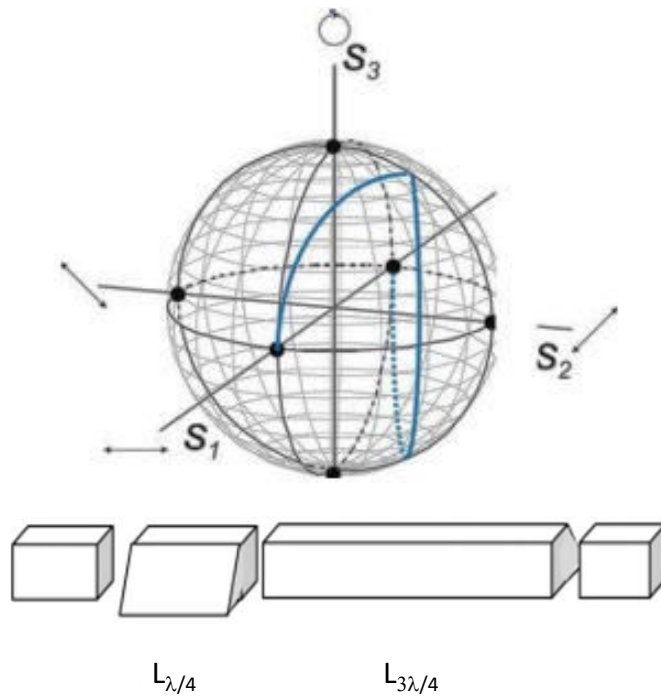


Figure 11.16: Upper: Trajectory of the SOP for conversion of TE to TM on the Poincaré sphere for the double section tolerant polarization converter. The dotted trajectory is at the backside of the sphere. Lower: Construction of a tolerant polarization converter. For clarity some space is left between the different sections, which in reality will not be there. Input and output waveguides, as well as the two mirrored converter sections, are shown.

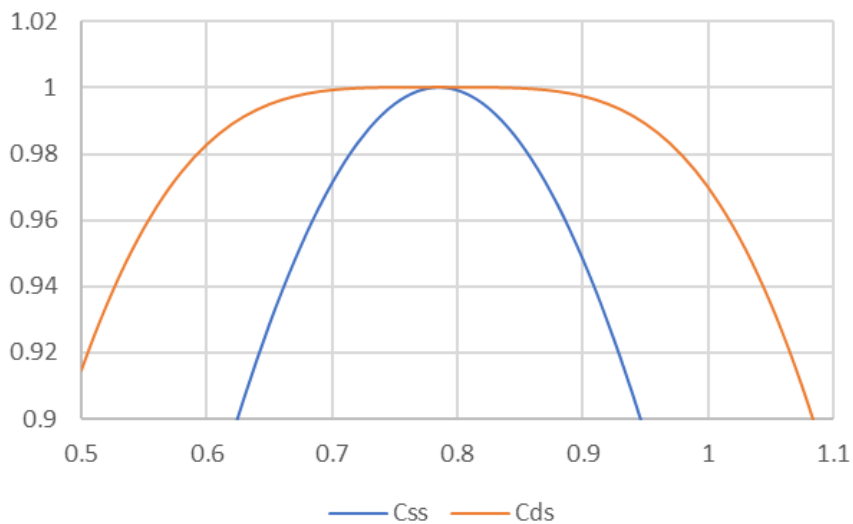


Figure 11.17: Conversion efficiency as a function of the tilting angle θ when the phase shift angle is π radians, for the single section (C_{SS}) and the double section (C_{DS}) device.

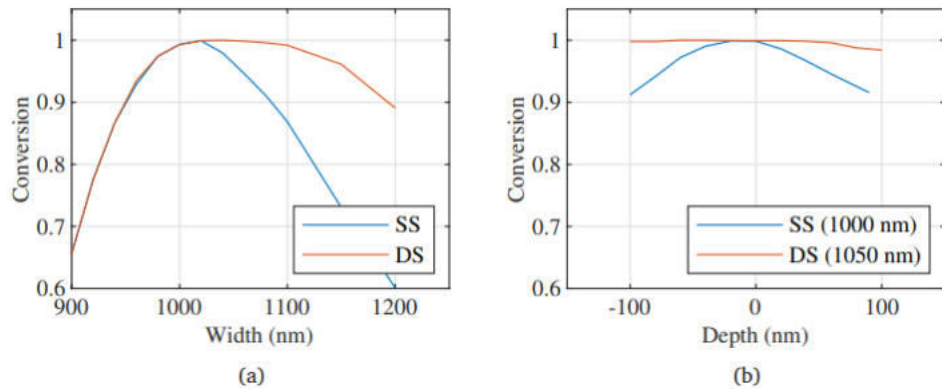


Figure 11.18: Simulated Conversion of Single Section (SS) and Double Section (DS) devices as a function of conversion section width (a) and etch depth (b).

be compensated for relatively large deviations. In order to investigate the tolerance of the double section device, we simulate the effect of width and depth deviations on the conversion of the device introduced in Fig. 11.11. Fig. 11.18 shows the conversion for both a single and a double section polarization converter.

It is seen that for the double section device plateaus appear, indicating that there is a wide width and depth range for which a high conversion can be obtained. If a width range of 100 nm is considered, the single section device would have a conversion above 94%, but the two section device would show a conversion >99% for this range. For applications where a 95% conversion efficiency is sufficient [182] the figure shows that the width tolerance of the two-section polarization converter is doubled with respect to the single section converter.

The width tolerance region is especially extended to the positive side, i.e., for wider converters, while for narrower converters the improvement is absent. The reason for this becomes clear from Fig. 11.13. For narrower converters the error in phase angle ϕ comes into play. As the tolerance improvement depends on compensating the tilting angle error $\Delta\theta$, the region where $\Delta\phi$ has limited influence (for wider converters) shows the best behavior. The designer can make use of this by designing the width for the two section polarization converter a bit larger, in order to aim for the middle of the plateau. This is applied in the simulations on the etch depth dependence [Fig. 11.18(b)], where the DS-device is chosen 50 nm wider than the SS-device. It is seen from these simulations that the double section polarization converter is virtually independent of the etch depth for this design, while the single section devices needs a control of better than ± 100 nm to obtain a reasonable conversion.

The performance of the polarization converters is also determined by other fabrication errors, such as deviations in material composition and layer thicknesses, as well as by deviations in the operational conditions assumed in the design. The ideas explained above can be used to improve tolerance in those parameters as well. This is illustrated with the wavelength dependence of the single section and the double section devices in Fig. 11.19.

Also in this case for the double section polarization converter a plateau is obtained, indicating that here too the error in the tilting angle is corrected. The wavelength dependence almost disappears for the DS-device. For the important C-band the original SS polarization converter gives above 95% conversion, but the new tolerant device promises 99.9%. This indicates that the performance of the converter improves

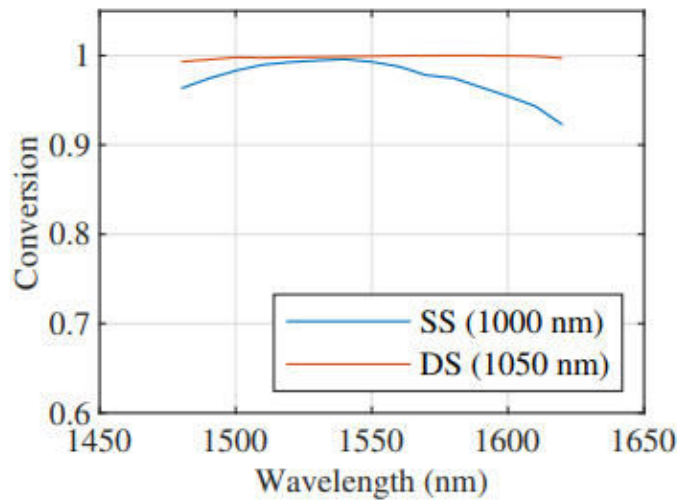


Figure 11.19: Wavelength dependence of single section (SS) and double section (DS) devices.

dramatically, supporting applications in which polarization purity is important, like polarization multiplexing or polarization switching. The simulated total loss, due to coupling between the different sections, is 0.5 dB.

11.6 Summary and Conclusions

This chapter introduces the effects of polarization on the operation of PICs. It identifies causes of polarization dependence and describes the influence on guided modes. Furthermore, the major device to manipulate the polarization state, the polarization converter, is explained. It is shown that waveguide birefringence in a waveguide with an asymmetric shape, where one of the sidewalls is sloped, can result in the guided wave analogon of a retardation plate. The theory for the polarization converter is given, and the technological steps needed for realization are described. Special attention is paid to fabrication tolerances of such a polarization converter. The major origin of the limited tolerances in the fabrication of single section sloped side polarization converters is identified to be the difficulty in maintaining a 45° tilting angle for the modes in the converter waveguide.

A new polarization converter is proposed to correct for deviations in this angle. It is a two section device, in which the two sections have modes with opposite tilting angles. The two sections are mirrored with respect to each other. This should be easily achievable in fabrication. The new two-section device shows a doubled width tolerance and wavelength range for more than 95% conversion, and yields significantly higher conversion efficiencies. The tolerant polarization converter has twice the length of the single-section device, and includes one extra waveguide junction. The junction losses in these devices can be kept low with an optimized design. The use of the polarization converter, and other polarization manipulating devices, in actual circuits is treated in chapter 27.

11.7 Appendices⁴⁵

Appendix 11A Jones calculus

R. Clark Jones introduced a vector-based description of polarization [184]. Write down the E_x and E_y waves as:

$$\begin{bmatrix} E_x \\ E_y \end{bmatrix} = \begin{bmatrix} E_{0x} \cos(kz - \omega t) \\ E_{0y} \cos(kz - \omega t + \phi) \end{bmatrix} \quad (11.15)$$

or in the complex form:

$$\begin{bmatrix} E_x \\ E_y \end{bmatrix} = \begin{bmatrix} E_{0x} e^{i(kz - \omega t)} \\ E_{0y} e^{i(kz - \omega t + \phi)} \end{bmatrix} \quad (11.16)$$

Get rid of the common wave term with $kz - \omega t$:

$$J = \begin{bmatrix} E_{0x} \\ E_{0y} e^{i\phi} \end{bmatrix} \quad (11.17)$$

This is the Jones vector of an elliptic state of polarization.

The Jones vectors of the linear and circular states are as follows. For the linear state, the phase difference between the E_x and E_y waves is πm . Division of last equation by $\sqrt{(E_{0x}^2 + E_{0y}^2)}$ gives the normalized Jones vector:

$$\bar{J} = \begin{bmatrix} \cos(\theta) \\ \sin(\theta) \end{bmatrix} \quad (11.18)$$

Then the normalized Jones vectors of the horizontal linear state \bar{J}_H and vertical linear state \bar{J}_V are:

$$\bar{J}_H = \begin{bmatrix} 1 \\ 0 \end{bmatrix}$$

$$\bar{J}_V = \begin{bmatrix} 0 \\ 1 \end{bmatrix}$$

the normalized Jones vectors of the $+45^\circ$ linear state \bar{J}_{45} and the -45° linear state \bar{J}_{-45} are:

$$\bar{J}_{45} = \frac{1}{\sqrt{2}} \begin{bmatrix} 1 \\ 1 \end{bmatrix}$$

$$\bar{J}_{-45} = \frac{1}{\sqrt{2}} \begin{bmatrix} 1 \\ -1 \end{bmatrix}$$

⁴Appendices A and B are based on sections 2.1.3 to 2.1.5 of the PhD Thesis of Dmitry Dzibrou.[183]

⁵Appendices C and D are based on Appendix A3 and section 2.2 of the PhD Thesis of Luc Augustin.[161]

We get the normalized Jones vectors of the right circular state \bar{J}_R and the left circular state \bar{J}_L in a similar way. The vectors are :

$$\bar{J}_{45} = \frac{1}{\sqrt{2}} \begin{bmatrix} 1 \\ i \end{bmatrix}$$

$$\bar{J}_V = \frac{1}{\sqrt{2}} \begin{bmatrix} 1 \\ -i \end{bmatrix}$$

Each of the three combinations of normalized Jones vectors of the polarization states above constitutes a representation basis of a polarization state. These three orthogonal bases can be converted into each other with a straightforward matrix multiplication. The beauty of the Jones vectors is that they can describe the evolution of a polarization state when light passes through a component in an optical system. Each component gets a 2×2 Jones matrix. Then to find the state of polarization at the output of the system, we only need to multiply the Jones vector of the input state of polarization by the matrixes of the components.

Appendix 11B Stokes parameters

The Jones calculus describes polarization using complex amplitudes. The problem of this description is that we cannot measure the amplitudes (and the phases) directly. The direct measurement is a measurement of power. In 1892, George Gabriel Stokes introduced a set of parameters that allows finding the state of polarization from measurements of light powers. Starting with the familiar two orthogonal plane waves E_x and E_y :

Stokes parameters

$$\begin{aligned} E_x &= E_{0x} \cos(kz - \omega t) \\ E_y &= E_{0y} \cos(kz - \omega t + \phi) \end{aligned} \quad (11.19)$$

With some algebra these plane waves lead to the equation of the polarization ellipse. To relate the equation of the polarization ellipse to powers, we average over time:

$$\frac{\langle E_x^2 \rangle}{E_{0x}^2} + \langle \frac{E_y^2}{E_{0y}^2} - \frac{2\langle E_x E_y \rangle}{E_{0x} E_{0y}} \cos \phi = \sin^2 \phi$$

where $\langle \dots \rangle$ is an averaged quantity. Multiplying this equation with $4E_{0x}^2 E_{0y}^2$ leads to:

$$4E_{0y}^2 \langle E_x^2 \rangle + 4E_{0x}^2 \langle E_y^2 \rangle - 8E_{0x} E_{0y} \langle E_x E_y \rangle \cos \phi = (2E_{0x} E_{0y} \sin \phi)^2$$

Since the averaging of the square of a cosine is $1/2$, the expressions for the plane waves tell us that

$$\begin{aligned} \langle E_x^2 \rangle &= \frac{1}{2} E_{0x}^2 \\ \langle E_y^2 \rangle &= \frac{1}{2} E_{0y}^2 \\ \langle E_x E_y \rangle &= \frac{1}{2} E_{0x} E_{0y} \cos \phi \end{aligned}$$

Combining the last 4 equations gives after rearrangement:

$$(E_{0x}^2 + E_{0y}^2)^2 = (E_{0x}^2 - E_{0y}^2)^2 + (2E_{0x} E_{0y} \cos \phi)^2 + (2E_{0x} E_{0y} \sin \phi)^2$$

This equation is very interesting: it suggests that we can relate the total power of light to the special cases of the elliptic state of polarization. We can write the equation also as:

$$S_0^2 = S_1^2 + S_2^2 + S_3^2$$

With the Stokes parameters defined as:

$$\begin{aligned} S_0 &= E_{0x}^2 + E_{0y}^2 \\ S_1 &= E_{0x}^2 - E_{0y}^2 \\ S_2 &= 2E_{0x}E_{0y} \cos \phi \\ S_3 &= 2E_{0x}E_{0y} \sin \phi \end{aligned}$$

Now look closer at the parameters. S_0 is the total power. S_1 is the difference in power between the horizontal linear state and the vertical linear state. To understand the last two parameters, we go back to the Jones vectors. The elliptic state of polarization is

$$J = \begin{bmatrix} E_{0x} \\ E_{0y}e^{i\phi} \end{bmatrix}$$

This Jones vector says that the elliptic state is a sum of the horizontal and the vertical linear states

$$J = \begin{bmatrix} E_{0x} \\ 0 \end{bmatrix} + \begin{bmatrix} 0 \\ E_{0y}e^{i\phi} \end{bmatrix}$$

and these two states are similar to the normalized Jones vectors of the horizontal linear J_H and the vertical linear J_V states. As mentioned in Appendix A it is also possible to represent the Jones vector of an elliptic state of polarization either with the $\pm 45^\circ$ linear states, or with the left and right circular states. To describe the Jones vector of the elliptic state using the $\pm 45^\circ$ linear states as a basis, we multiply with the appropriate matrix to obtain:

$$J_{B45} = \frac{1}{\sqrt{2}} \begin{bmatrix} E_{0x}e^{-i\phi/2} + E_{0y}e^{i\phi/2} \\ E_{0x}e^{-i\phi/2} - E_{0y}e^{i\phi/2} \end{bmatrix} = \begin{bmatrix} E_{45} \\ E_{-45} \end{bmatrix}$$

where J_{B45} is the Jones vector of the elliptic state of polarization described with the basis of $\pm 45^\circ$ linear states. The difference in powers between the $\pm 45^\circ$ -states is

$$P_{45} - P_{-45} = 2E_{0x}E_{0y} \cos \phi$$

and this is the S_2 Stokes parameter. Similarly, we can describe the Jones vector of the elliptic state using the right and left circular state. Then we find:

$$J_{BRL} = \frac{1}{\sqrt{2}} \begin{bmatrix} E_{0x}e^{-i\phi/2} - E_{0y}e^{i\phi/2} \\ E_{0x}e^{-i\phi/2} + E_{0y}e^{i\phi/2} \end{bmatrix} = \begin{bmatrix} E_L \\ E_R \end{bmatrix}$$

where J_{BRL} is the Jones vector described with the basis of left and right circular states, E_L is the electric field of the left circular state and E_R is the electric field of the right circular state. The power difference between the left and right circular states is

$$P_L - P_R = 2E_{0x}E_{0y} \sin \phi$$

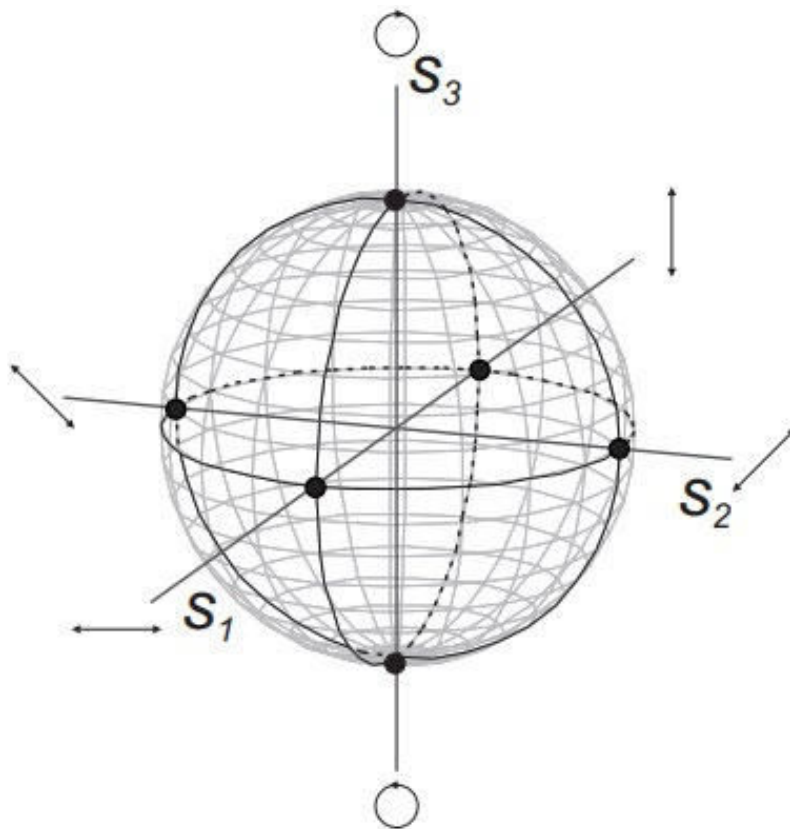


Figure 11.20: Poincaré sphere for visualizing the state of polarization.

and this difference is the S_3 Stokes parameter. We see that the Stokes parameters relate to measurable quantities: powers. Together they define the state of polarization. The parameter S_0 , which represents the power of the optical wave, can be used to normalize the other Stokes parameters. The three normalized Stokes parameters can be regarded as vector components, thus leading to the Stokes vector. It has a unit length in a three dimensional space, so each vector represents a state of polarization as a point on a sphere with a unity radius. And that is what the French mathematician Henri Poincaré understood.

Stokes vector

Appendix 11C Poincaré sphere

A visual interpretation of the normalized Stokes parameters can be obtained by plotting them as coordinates on a sphere with radius 1. From this representation the SOP can be easily observed. Points on the poles of this Poincaré sphere (Fig. 11.20) correspond to circularly polarized light: left-handed circular at the south pole, right-handed at the north pole. At the equator the light is linearly polarized, at the intersection with the S_1 -axis it is fully TE or TM-polarized. At the nearer point, $S_1 = 1$, it is TE-polarized (0°). The further point, $S_1 = -1$, indicates TM (90°) polarized light. The left and right intersections with the S_2 -axis are the points in which the light has an equal amount of TE and TM polarized light ($\pm 45^\circ$). The areas between the poles and the equator describe various elliptical polarization states.

Poincaré sphere

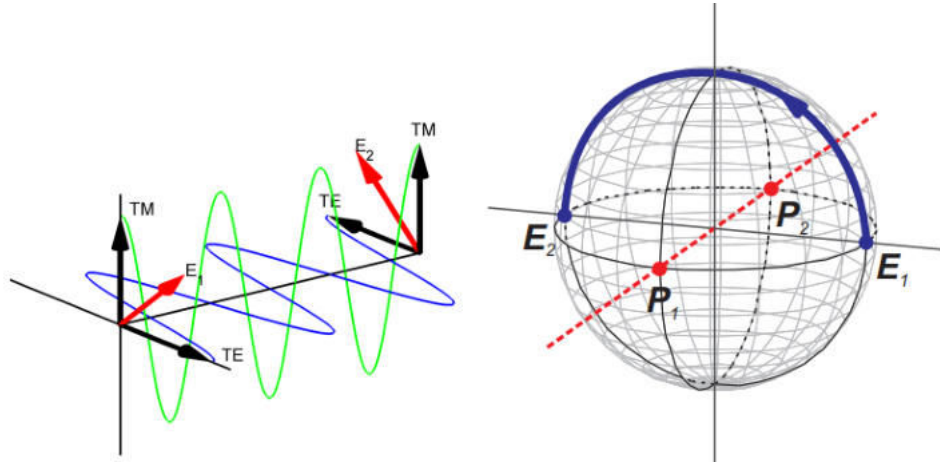


Figure 11.21: The change of the polarization when π phaseshift is applied. Left: Propagation. Right: Poincaré sphere.

The sphere is very well suited for showing the change in polarization, if the light travels through a photonic device. This is explained by the example of a polarization-dependent phase shift in a waveguide into which 45° linearly polarized light is fed. The light incident into the waveguide (E_1) can be decomposed into the two orthogonal stable polarization modes present inside the waveguide: P_1 and P_2 , in this case TE and TM, respectively, as indicated in Fig. 11.21(right). The change in polarization is calculated using the Jones matrix of the phase shifter and is plotted on a Poincaré sphere. The normalized input polarization is:

$$E_1 = \frac{1}{\sqrt{2}} \begin{bmatrix} 1 \\ 1 \end{bmatrix}$$

The transfer matrix of the waveguide employing $\Delta\phi$ phase shift is given by:

$$T = \begin{bmatrix} e^{j\Delta\phi} & 0 \\ 0 & 1 \end{bmatrix} \quad (11.20)$$

The output polarization E_2 is obtained from the matrix multiplication:

$$E_2 = TE_1 = \frac{1}{\sqrt{2}} \begin{bmatrix} e^{j\Delta\phi} \\ 1 \end{bmatrix}$$

Fig. 11.21(left) shows the propagation of the modes through the device. The corresponding Poincaré sphere is plotted in Fig. 11.21(right). Those two modes correspond to two points on the sphere, opposite to each other. While propagating through the structure, phase differences between these two stable modes (P_1 and P_2) occur, which is equivalent to rotating around the axis through these modes. So a phase shift of π translates to a rotation of π radians around the S_1 -axis. The calculation and visualization methods discussed here are used to describe the polarization behaviour of optical components in PICs. More details can be found in [111, 112, 113].

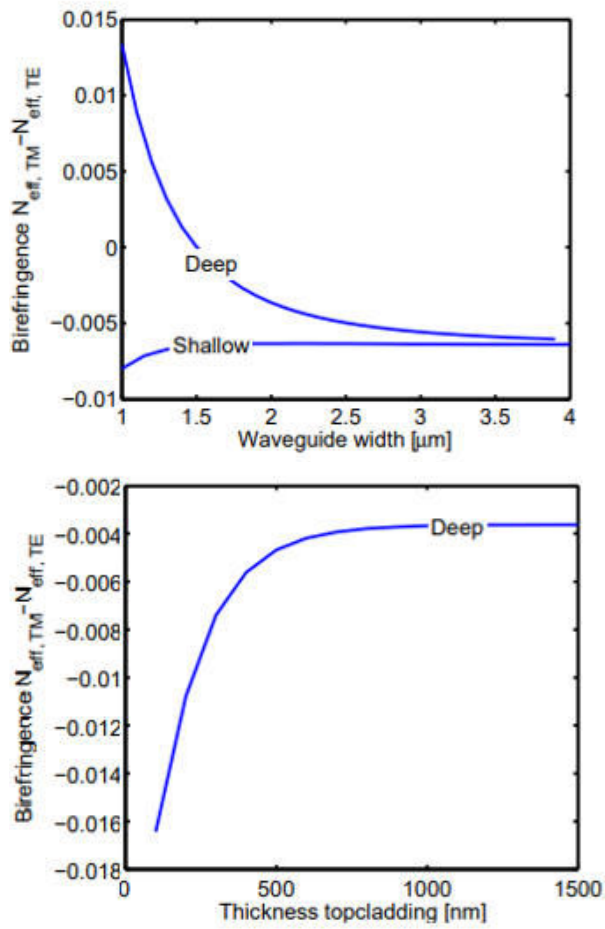


Figure 11.22: Modal birefringence as a function of width (top) and top cladding (bottom)

Appendix 11D Modal birefringence

Given a certain material refractive index (and birefringence, the difference Δn in the refractive indices), the modal birefringence can be designed. The birefringence depends on the geometry of the waveguide, especially on the width and the thickness of the top cladding.

The birefringence in the waveguide can be calculated with a mode solver, e.g., using the Film Mode Matching method [181]. The birefringence as a function of width for a wavelength of 1555 nm is plotted in Fig. 11.22(left) for both deep and shallow waveguides. For deep waveguides, the birefringence is 0 for a width of 1.5 μm . A polarization independent waveguide can be obtained for this width, but the slope of the tangent at this point is steep, so the tolerance in width is very small.

In contrast to a deep waveguide, the birefringence in a shallow waveguide is small and cannot be influenced much by changing the width and no polarization independent waveguide can be obtained in this case. In Fig. 11.22(right) the birefringence as a function of the top cladding thickness is shown for a 2 μm wide deep waveguide. The birefringence is largest for a thin cladding, as the air-semiconductor boundary is close to the field in that case. For a thickness above 600 nm the birefringence remains constant. If high birefringence is needed, a thin top cladding is preferred. Narrowing the waveguides will increase the birefringence, but will also decrease the width tolerances.

The birefringence has a dispersive nature, which has to be taken into account when operation over a wide wavelength range is required. The material dispersion and refractive indices [119] as well as the dispersion of the modal birefringence are plotted in Fig. 11.23.

The dispersion of the birefringence is largest for narrow waveguides and approaches 0 for waveguides wider than 3 μm . It should be noted that for waveguides with widths around 1.5 μm , the birefringence changes sign around 1540 nm. So for shorter wavelengths $N_{\text{eff, TM}} > N_{\text{eff, TE}}$, while for longer wavelengths $N_{\text{eff, TE}}$ is larger. It is important to take this into account if the phase difference is used for the function of a device, e.g., in the polarization splitter demonstrated in chapter 27.

Material birefringence The modal birefringence can also be influenced by material birefringence. Material birefringence is caused by a different material refractive index for different orientations of the polarization. In InP/InGaAsP this phenomenon is in principle absent, but it can occur due to e.g. photo-elastic and electro-optic effects. In a passive waveguide, only the photo-elastic effect can cause material birefringence. The material birefringence is influenced by strain, introduced in the growth. The birefringence for quaternary material grown on (100) InP substrate is linearly dependent on the strain. The difference between refractive indices parallel (for TE-polarized light) and perpendicular (for TM-polarized light) to the interface of the layers can be calculated [185] from the strain in the material, the elastic compliance tensor, and the linear photo-elastic coefficient [186]. The resulting material birefringence for Q(1.25) as a function of the strain is plotted in Fig. 11.24(left). The birefringence is positive ($n_{\text{TM}} > n_{\text{TE}}$) for tensile and negative for compressive strain.

These results are used to calculate the influence of strain on the modal birefringence. For a typical value of 0.04% tensile strain, the modal birefringence is calculated as a function of width for deep waveguides. This is plotted in Fig. 11.24(right). For narrow widths, the additional material birefringence has only a small influence on the modal birefringence; the confinement because of the geometry of the waveguide plays a larger role. For wider waveguides the material birefringence is more important. Nar-

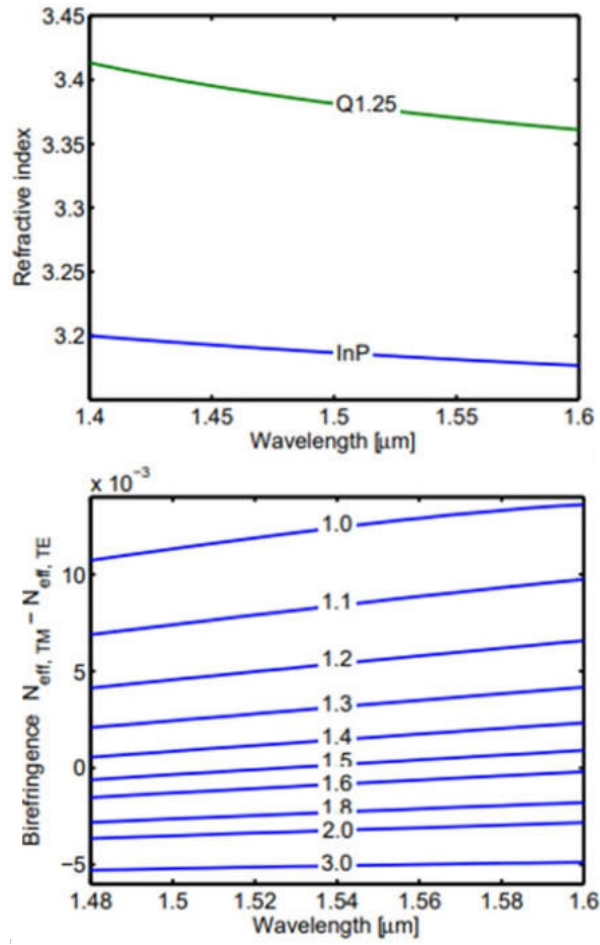


Figure 11.23: Material dispersion (top) and calculated effective index difference between TE and TM (bottom) as a function of wavelength for different waveguide widths.

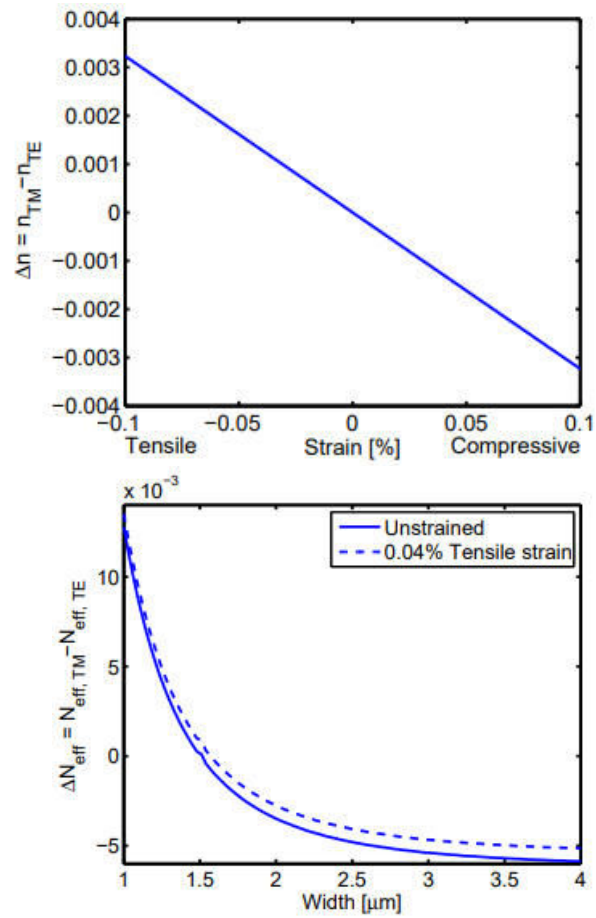


Figure 11.24: Top: Material birefringence of strained Q(1.25) InP as a function of strain. Bottom: Modal birefringence of 0.04% on tensile strained compared to unstrained Q(1.25).

row waveguides are preferred for a device tolerant to strain in the material, but wide waveguides show a more width-tolerant birefringence. This is a trade-off that has to be made depending on the requirements for a device.